Population-specific causal disease effect sizes in functionally important regions impacted by selection

Huwenbo Shi[1,2,*], Steven Gazal[1,2], Masahiro Kanai[2,3,4,5,6], Evan M. Koch[7,8], Armin P. Schoech[1,2,9], Samuel S. Kim[1,2,10], Yang Luo[2,5,7,11,12], Tiffany Amariuta[2,5,11,12,13], Yukinori Okada[6,14], Soumya Raychaudhuri[2,5,7,11,12,15], Shamil R. Sunyaev[7,8], and Alkes L. Price[1,2,9,†]

[1]Department of Epidemiology, Harvard T.H. Chan School of Public Health, Boston, MA, USA
[2]Program in Medical and Population Genetics, Broad Institute of MIT and Harvard, Cambridge, MA, USA
[3]Analytic and Translational Genetics Unit, Massachusetts General Hospital, Boston, MA, USA
[4]Stanley Center for Psychiatric Research, Broad Institute of Harvard and MIT, Cambridge, MA, USA
[5]Department of Biomedical Informatics, Harvard Medical School, Boston, MA, USA
[6]Department of Statistical Genetics, Osaka University Graduate School of Medicine, Suita, Japan
[7]Division of Genetics, Brigham and Women's Hospital, Harvard Medical School, Boston, MA, USA
[8]Department of Medicine, Harvard Medical School, Boston, MA, USA
[9]Department of Biostatistics, Harvard T.H. Chan School of Public Health, Boston, MA, USA
[10]Department of Electrical Engineering and Computer Science, Massachusetts Institute of Technology, Cambridge, MA, USA
[11]Division of Rheumatology, Immunology, and Allergy, Brigham and Women's Hospital, Harvard Medical School, Boston, MA, USA
[12]Center for Data Sciences, Brigham and Women's Hospital, Harvard Medical School, Boston, MA, USA
[13]Graduate School of Arts andSciences, Harvard University, Cambridge, MA, USA
[14]Laboratory of Statistical Immunology, Immunology Frontier Research Center (WPI-IFReC), Osaka University, Suita, Japan
[15]Arthritis Research UK Centre for Genetics and Genomics, Centre for Musculoskeletal Research, Manchester Academic Health Science Centre, The University of Manchester, Manchester, UK

Correspondence: *hshi@hsph.harvard.edu (HS), †aprice@hsph.harvard.edu (ALP)

Abstract

Many diseases and complex traits exhibit population-specific causal effect sizes with trans-ethnic genetic correlations significantly less than 1, limiting trans-ethnic polygenic risk prediction. We developed a new method, S-LDXR, for stratifying squared trans-ethnic genetic correlation across genomic annotations, and applied S-LDXR to genome-wide association summary statistics for 30 diseases and complex traits in East Asians (EAS) and Europeans (EUR) (average N_{EAS}=93K, N_{EUR}=274K) with an average trans-ethnic genetic correlation of 0.83 (s.e. 0.01). We determined that squared trans-ethnic genetic correlation was $0.81\times$ (s.e. 0.01) smaller than the genome-wide average at SNPs in the top quintile of background selection statistic, implying more population-specific causal effect sizes. Accordingly, causal effect sizes were more population-specific in functionally important regions, including coding, conserved, and regulatory regions. In analyses of regions surrounding specifically expressed genes, causal effect sizes were most population-specific for skin and immune genes and least population-specific for brain genes. Our results could potentially be explained by stronger gene-environment interaction at loci impacted by selection, particularly positive selection.

Introduction

Trans-ethnic genetic correlations are significantly less than 1 for many diseases and complex traits,[1–6] implying that population-specific causal disease effect sizes contribute to the incomplete portability of genome-wide association study (GWAS) findings and polygenic risk scores to non-European populations.[6–12] However, current methods for estimating genome-wide trans-ethnic genetic correlations assume the same trans-ethnic genetic correlation for all categories of SNPs,[2,5,13] providing little insight into why causal disease effect sizes are population-specific. Understanding the biological processes contributing to population-specific causal disease effect sizes can help inform polygenic risk prediction in non-European populations and alleviate health disparities.[6,14,15]

Here, we introduce a new method, S-LDXR, for stratifying squared trans-ethnic genetic correlation across functional categories of SNPs using GWAS summary statistics and population-matched linkage disequilibrium (LD) reference panels (e.g. the 1000 Genomes Project[16]); we stratify the *squared* trans-ethnic genetic correlation across functional categories to robustly handle noisy heritability estimates. We confirm that S-LDXR yields robust estimates in extensive simulations. We apply S-LDXR to 30 diseases and complex traits with GWAS summary statistics available in both East Asian (EAS) and European (EUR) populations, leveraging recent large studies in East Asian populations from the CONVERGE consortium and Biobank Japan;[17–19] we analyze a broad set of genomic annotations from the baseline-LD model,[20–22] as well as tissue-specific annotations based on specifically expressed gene sets.[23]

Results

Overview of methods

Our method (S-LDXR) for estimating stratified trans-ethnic genetic correlation is conceptually related to stratified LD score regression[20,21] (S-LDSC), a method for partitioning heritability from GWAS summary statistics. The S-LDSC method determines that a category of SNPs is enriched for heritability if SNPs with high LD to that category have higher expected χ^2 statistic than SNPs with low LD to that category. Analogously, the S-LDXR method determines that a category of SNPs is enriched for trans-ethnic genetic covariance if SNPs with high LD to that category have higher expected product of Z-scores than SNPs with low LD to that category. Unlike S-LDSC, S-LDXR models per-allele effect sizes (accounting for differences in minor allele frequency (MAF) between populations), and employs a shrinkage estimator to reduce noise.

In detail, the product of Z-scores of SNP j in two populations, $Z_{1j}Z_{2j}$, has the expectation

$$\mathrm{E}[Z_{1j}Z_{2j}] = \sqrt{N_1 N_2} \sum_C \ell_\times(j, C)\theta_C \; , \tag{1}$$

where N_p is the sample size for population p; $\ell_\times(j, C) = \sum_k r_{1jk}r_{2jk}\sigma_{1j}\sigma_{2j}a_C(k)$ is the trans-ethnic LD score of SNP j with respect to annotation C, whose value for SNP k, $a_C(k)$, can be either binary or continuous; r_{pjk} is the LD (Pearson correlation) between SNP j and k in population p; σ_{pj} is the standard deviation of SNP j genotypes in population p; and θ_C represents the per-SNP contribution to trans-ethnic genetic covariance of the *per-allele* causal disease effect size of annotation C. Here, r_{pjk} and σ_{pj} can be estimated from population-matched reference panels (e.g. 1000 Genomes Project[16]). We estimate θ_C for each annotation C using weighted least square regression. Subsequently, we estimate the trans-ethnic genetic covariance of each binary annotation C ($\rho_g(C)$) as $\sum_{j\in C} \sum_{C'} a_{C'}(j)\theta_{C'}$, using coefficients ($\theta_{C'}$) for both binary and continuous-valued annotations C'; the heritabilities in each population ($h_{g1}^2(C)$ and $h_{g2}^2(C)$) are estimated analogously. We then estimate the stratified *squared* trans-ethnic genetic correlation, defined as

$$r_g^2(C) = \frac{\rho_g^2(C)}{h_{g1}^2(C)h_{g2}^2(C)} \; . \tag{2}$$

In this work, we only estimate $r_g^2(C)$ for SNPs with MAF greater than 5% in both populations. We estimate $r_g^2(C)$ instead of $r_g(C)$ to avoid bias (or undefined values) from computing square roots of noisy (possibly negative) heritability estimates, and use a boot-

4

97 strap method[24] to correct for bias in estimating a ratio. We further employ a shrinkage
98 estimator, with shrinkage parameter α (between 0 and 1, where larger values imply more
99 shrinkage; the default value is 0.5), to reduce noise. We do not constrain estimates of $r_g^2(C)$
100 to their plausible range (between 0 and 1), which would introduce bias. We define the en-
101 richment/depletion of squared trans-ethnic genetic correlation as $\lambda^2(C) = \frac{r_g^2(C)}{r_g^2}$, where r_g^2
102 is the genome-wide squared trans-ethnic genetic correlation; $\lambda^2(C)$ can be meta-analyzed
103 across traits with different r_g^2. We compute standard errors via block-jackknife, as in previ-
104 ous work.[20] We estimate $\lambda^2(C)$ for binary annotations only, such as functional annotations[20]
105 or quintiles of continuous-valued annotations.[21] Further details of the S-LDXR method are
106 provided in the Methods section; we have publicly released open-source software implement-
107 ing the method (see URLs). We note that all genetic correlations are defined using *causal*
108 effect sizes, as opposed to joint-fit effect sizes.[2,5]

109   We apply S-LDXR to 62 annotations, defined in both EAS and EUR populations (Table
110 S1, Figure S1, S2). 61 of these annotations (54 binary annotations and 7 continuous-valued
111 annotations) are from the baseline-LD model (v1.1; see URLs), which includes a broad set
112 of coding, conserved, regulatory and LD-related annotations; we modified the definition of
113 two MAF-adjusted continuous-valued annotations (level of LD (LLD) and predicted allele
114 age) to make them compatible with both populations. We also added one new continuous-
115 valued annotation, SNP-specific F_{ST} between EAS and EUR populations. We did not include
116 MAF bins from the baseline-LD model, due to the complexity of defining MAF bins in both
117 populations. We refer to our final set of annotations as the baseline-LD-X model (Methods).
118 We have publicly released all baseline-LD-X model annotations and LD scores for EAS
119 and EUR populations (see URLs). We also apply S-LDXR to specifically expressed gene
120 annotations for 53 tissues[23] (Table S2).

Simulations

122   We evaluated the accuracy of S-LDXR in simulations using genotypes that we sim-
123 ulated using HAPGEN2[25] from phased haplotypes of 481 EAS and 489 EUR individuals
124 from the 1000 Genomes Project[16] (35,378 simulated EAS-like and 36,836 simulated EUR-
125 like samples, after removing genetically related samples; $\sim$2.5 million SNPs on chromosomes
126 1 − 3) (Methods); we did not have access to individual-level EAS data at sufficient sam-
127 ple size to perform simulations with real genotypes. For each population, we randomly
128 selected a subset of 500 simulated samples to serve as the reference panel for estimating LD
129 scores. We performed both null simulations (heritable trait with functional enrichment but
130 no enrichment/depletion of squared trans-ethnic genetic correlation; $\lambda^2(C) = 1$) and causal

₁₃₁ simulations ($\lambda^2(C) \neq 1$). In our main simulations, we randomly selected 10% of the SNPs as

₁₃₂ causal SNPs in both populations, set genome-wide heritability to 0.5 in each population, and

₁₃₃ adjusted genome-wide genetic covariance to attain a genome-wide r_g of 0.60 (unless otherwise

₁₃₄ indicated). In the null simulations, we used heritability enrichments from analyses of real

₁₃₅ traits in EAS samples to specify per-SNP causal effect size variances and covariances. In the

₁₃₆ causal simulations, we directly specified per-SNP causal effect size variances and covariances

₁₃₇ to attain $\lambda^2(C) \neq 1$ values from analyses of real traits, as these were difficult to attain using

₁₃₈ the heritability and trans-ethnic genetic covariance enrichments from analyses of real traits.

₁₃₉ First, we assessed the accuracy of S-LDXR in estimating genome-wide trans-ethnic ge-

₁₄₀ netic correlation (r_g). Across a wide range of simulated r_g values (0.20 to 0.96), S-LDXR

₁₄₁ yielded approximately unbiased estimates and well-calibrated jackknife standard errors (Ta-

₁₄₂ ble S3, Figure S3).

₁₄₃ Second, we assessed the accuracy of S-LDXR in estimating $\lambda^2(C)$ in quintiles of the 8

₁₄₄ continuous-valued annotations of the baseline-LD-X model. We performed both null sim-

₁₄₅ ulations ($\lambda^2(C) = 1$) and causal simulations ($\lambda^2(C) \neq 1$). Results are reported in Figure

₁₄₆ 1a and Tables S4 – S9 . At default parameter settings, S-LDXR yielded approximately un-

₁₄₇ biased estimates of $\lambda^2(C)$ for most annotations. As a secondary analysis, we tried varying

₁₄₈ the S-LDXR shrinkage parameter, α, which has a default value of 0.5. We determined that

₁₄₉ reducing the shrinkage parameter led to less accurate estimates of $\lambda^2(C)$ for annotations

₁₅₀ depleted for heritability, whereas increasing the shrinkage parameter biased results towards

₁₅₁ $\lambda^2(C) = 1$ in causal simulations (Figure S4, Tables S5, S8). Results were similar at other

₁₅₂ values of the proportion of causal SNPs (1% and 100%; Tables S4, S6, S7, S9). We also

₁₅₃ confirmed that S-LDXR produced well-calibrated jackknife standard errors (Tables S4-S9).

₁₅₄ Finally, we assessed the accuracy of S-LDXR in estimating $\lambda^2(C)$ for the 28 main binary

₁₅₅ annotations of the baseline-LD-X model (inherited from the baseline model of ref.[20]). We

₁₅₆ discarded $\lambda^2(C)$ estimates with the highest standard errors (top 5%), as estimates with large

₁₅₇ standard errors (which are particularly common for annotations of small size) are uninfor-

₁₅₈ mative for evaluating unbiasedness of the estimator (in analyses of real traits, trait-specific

₁₅₉ estimates with large standard errors are retained, but contribute very little to meta-analysis

₁₆₀ results). Results are reported in Figure 1b and Tables S5, S8. At default parameter settings,

₁₆₁ S-LDXR yielded approximately unbiased estimates of $\lambda^2(C)$ for functional annotations of

₁₆₂ large size in both null and causal simulations; however, estimates were slightly downward

₁₆₃ biased in null simulations for functional annotations of small size (e.g. 5' UTR; 0.5% of

₁₆₄ SNPs). This is likely because the bootstrap method for correcting bias in ratio estimation

₁₆₅ (Methods) has limited capability when heritability estimates in the denominator of Equa-

₁₆₆ tion (2) are noisy,[24] as is the case for small annotations. Increasing the shrinkage parameter

167 above its default value of 0.5 and extending the functional annotations by 500bp on each
168 side[20] ameliorated the downward bias (and reduced standard errors) for annotations of small
169 size in null simulations (Figure S5, S6);. However, increasing the shrinkage parameter also
170 biased results towards the null ($\lambda^2(C) = 1$) in causal simulations (Tables S7, S8, S9), and
171 $\lambda^2(C)$ estimates for the extended annotations are less biologically meaningful than for the
172 corresponding main annotations. To ensure robust estimates, we focus on the 20 main bi-
173 nary annotations of large size ($> 1\%$ of SNPs) in analyses of real traits (see below). Results
174 were similar at other values of the proportion of causal SNPs (1% and 100%; Tables S4, S6,
175 S7, S9). We also confirmed that S-LDXR produced well-calibrated jackknife standard errors
176 (Tables S4-S9).

177   In summary, S-LDXR produced approximately unbiased estimates of enrichment/depletion
178 of squared trans-ethnic genetic correlation in both null and causal simulations of both quin-
179 tiles of continuous-valued annotations and binary annotations of large size ($> 1\%$ of SNPs).

Analysis of baseline-LD-X model annotations across 30 diseases and complex traits

182   We applied S-LDXR to 30 diseases and complex traits with summary statistics in East
183 Asians (average N = 93K) and Europeans (average N = 274K) available from Biobank
184 Japan, UK Biobank, and other sources (Table S10 and Methods). First, we estimated the
185 trans-ethnic genetic correlation (r_g) (as well as population-specific heritabilies) for each trait.
186 Results are reported in Figure S7 and Table S10. The average r_g across 30 traits was 0.83
187 (s.e. 0.01) (average $r_g^2 = 0.69$ (s.e. 0.02)). 28 traits had $r_g < 1$, and 11 traits had r_g
188 significantly less than 1 after correcting for 30 traits tested ($P < 0.05/30$); the lowest r_g was
189 0.34 (s.e. 0.07) for Major Depressive Disorder (MDD), although this may be confounded by
190 different diagnostic criteria in the two populations.[26] These estimates were consistent with
191 estimates obtained using Popcorn[2] (Figure S8) and those reported in previous studies.[2,5,6]

192   Second, we estimated the enrichment/depletion of squared trans-ethnic genetic correla-
193 tion ($\lambda^2(C)$) in quintiles of the 8 continuous-valued annotations of the baseline-LD-X model,
194 meta-analyzing results across traits; these annotations are moderately correlated (Figure 2a
195 and Table S1). We used the default shrinkage parameter ($\alpha = 0.5$) in all analyses. Results
196 are reported in Figure 2b and Table S11. We consistently observed a depletion of $r_g^2(C)$
197 ($\lambda^2(C) < 1$, implying more population-specific causal effect sizes) in functionally important
198 regions. For example, we estimated $\lambda^2(C) = 0.81$ (s.e. 0.01) for SNPs in the top quintile of
199 background selection statistic (defined as $1 -$ McVicker B statistic / 1000;[27] see ref.[21]); $\lambda^2(C)$
200 estimates were less than 1 for 27/30 traits (including 7 traits with two-tailed $p < 0.05/30$).

7

The background selection statistic quantifies the genetic distance of a site to its nearest exon; regions with high background selection statistic have higher per-SNP heritability, consistent with the action of selection, and are enriched for functionally important regions.[21] We observed the same pattern for CpG content and SNP-specific F_{st} (which are positively correlated with background selection statistic; Figure 2a) and the opposite pattern for nucleotide diversity (which is negatively correlated with background selection statistic). We also estimated $\lambda^2(C) = 0.85$ (s.e. 0.03) for SNPs in the top quintile of average LLD (which is positively correlated with background selection statistic), although these SNPs have *lower* per-SNP heritability due to a competing positive correlation with predicted allele age.[21] Likewise, we estimated $\lambda^2(C) = 0.83$ (s.e. 0.02) for SNPs in the *bottom* quintile of recombination rate (which is negatively correlated with background selection statistic), although these SNPs have average per-SNP heritability due to a competing negative correlation with average LLD.[21] However, $\lambda^2(C) < 1$ estimates for the bottom quintile of GERP (NS) (which is positively correlated with both background selection statistic and recombination rate) and the middle quintile of predicted allele age are more difficult to interpret. For all annotations analyzed, heritability enrichments did not differ significantly between EAS and EUR, consistent with previous studies.[19,28] Results were similar at a more stringent shrinkage parameter value ($\alpha = 1.0$; Figure S9), and for a meta-analysis across a subset of 20 approximately independent traits (Methods; Figure S10).

Finally, we estimated $\lambda^2(C)$ for the 28 main binary annotations of the baseline-LD-X model (Table S1), meta-analyzing results across traits. Results are reported in Figure 3a and Table S12. Our primary focus is on the 20 annotations of large size ($> 1\%$ of SNPs), for which our simulations yielded robust estimates; results for remaining annotations are reported in Table S12. We consistently observed a depletion of $\lambda^2(C)$ (implying more population-specific causal effect sizes) within these annotations: 17 annotations had $\lambda^2(C) < 1$, and 8 annotations had $\lambda^2(C)$ significantly less than 1 after correcting for 20 annotations tested ($P < 0.05/20$); these annotations included Coding ($\lambda^2(C) = 0.90$ (s.e. 0.03)), Conserved ($\lambda^2(C) = 0.92$ (s.e. 0.02)), Promoter ($\lambda^2(C) = 0.88$ (s.e. 0.03)) and Super Enhancer ($\lambda^2(C) = 0.91$ (s.e. 0.01)), each of which was significantly enriched for per-SNP heritability, consistent with ref.[20] For all annotations analyzed, heritability enrichments did not differ significantly between EAS and EUR (Figure 3a), consistent with previous studies.[19,28] Results were similar at a more stringent shrinkage parameter value ($\alpha = 1.0$; Figure S9), and for a meta-analysis across a subset of 20 approximately independent traits (Methods; Figure S11).

Since the functional annotations are moderately correlated with the 8 continuous-valued annotations (Table S1c, Figure S1), we investigated whether the depletions of squared transethnic genetic correlation ($\lambda^2(C) < 1$) within the 20 binary annotations could be explained

237 by the 8 continuous-valued annotations. For each binary annotation, we estimated its ex-
238 pected $\lambda^2(C)$ based on values of the 8 continuous-valued annotations for SNPs in the binary
239 annotation (Methods), meta-analyzed this quantity across traits, and compared observed vs.
240 expected $\lambda^2(C)$ (Figure 3b and Table S13). We observed strong concordance, with a slope
241 of 0.63 (correlation of 0.56) across the 20 binary annotations. This implies that the deple-
242 tions of $r_g^2(C)$ ($\lambda^2(C) < 1$) within binary annotations are largely explained by corresponding
243 values of continuous-valued annotations.

244   In summary, our results show that causal disease effect sizes are more population-specific
245 in functionally important regions impacted by selection. Further interpretation of these
246 findings, including the role of positive and/or negative selection, is provided in the Discussion
247 section.

Analysis of specifically expressed gene annotations

249   We analyzed 53 specifically expressed gene (SEG) annotations, defined in ref.[23] as
250 ± 100kb regions surrounding the top 10% of genes specifically expressed in each of 53 GTEx[29]
251 tissues (Table S2), by applying S-LDXR with the baseline-LD-X model to the 30 diseases and
252 complex traits (Table S10). We note that although SEG annotations were previously used to
253 prioritize disease-relevant tissues based on disease-specific heritability enrichments,[19,23] en-
254 richment/depletion of squared trans-ethnic genetic correlation ($\lambda^2(C)$) is standardized with
255 respect to heritability, hence not expected to produce disease-specific signals. Thus, for each
256 tissue, we meta-analyzed $\lambda^2(C)$ estimates across the 30 diseases and complex traits.

257   Results are reported in Figure 4a and Table S14. $\lambda^2(C)$ estimates were less than 1 for
258 all 53 tissues and significantly less than 1 ($p < 0.05/53$) for 39 tissues, with statistically
259 significant heterogeneity across tissues ($p < 10^{-20}$; Methods). The strongest depletions of
260 squared trans-ethnic genetic correlation were observed in skin tissues (e.g. $\lambda^2(C) = 0.81$ (s.e.
261 0.02) for Skin Sun Exposed (Lower Leg)), Prostate and Ovary (e.g. $\lambda^2(C) = 0.82$ (s.e. 0.02)
262 for Prostate) and immune-related tissues (e.g. $\lambda^2(C) = 0.83$ (s.e. 0.02) for Spleen), and
263 the weakest depletions were observed in Testis ($\lambda^2(C) = 0.97$ (s.e. 0.02)) and brain tissues
264 (e.g. $\lambda^2(C) = 0.96$ (s.e. 0.02) for Brain Nucleus Accumbens (Basal Ganglia)). Results
265 were similar at less stringent and more stringent shrinkage parameter values ($\alpha = 0.0$ and
266 $\alpha = 1.0$; Figures S12, S13 and Table S14). A comparison of 14 blood-related traits and 16
267 other traits yielded highly consistent $\lambda^2(C)$ estimates ($R = 0.82$; Figure S14, Table S15),
268 confirming that these findings were not disease-specific.

269   These $\lambda^2(C)$ results were consistent with the higher background selection statistic[27] in
270 Skin Sun Exposed (Lower Leg) ($R = 0.17$), Prostate ($R = 0.16$) and Spleen ($R = 0.14$) as

9

271 compared to Testis ($R = 0.02$) and Brain Nucleus Accumbens (Basal Ganglia) ($R = 0.08$)
272 (Figure S15, Table S2), and similarly for CpG content (Figure S16, Table S2). Although
273 these results could in principle be confounded by gene size,[30] the low correlation between
274 gene size and background selection statistic ($R = 0.06$) or CpG content ($R = -0.20$) (in
275 $\pm$100kb regions) implies limited confounding. We note the well-documented action of recent
276 positive selection on genes impacting skin pigmentation[31–35] and the immune system;[31–34,36]
277 we are not currently aware of any evidence of positive selection impacting Prostate and
278 Ovary. We further note the well-documented action of negative selection on fecundity- and
279 brain-related traits,[37–39] but it is possible that recent positive selection may more closely
280 track differences in causal disease effect sizes across human populations, which have split
281 relatively recently[40] (see Discussion).

282 More generally, since SEG annotations are moderately correlated with the 8 continuous-
283 valued annotations (Figure S17, Table S2), we investigated whether these $\lambda^2(C)$ results could
284 be explained by the 8 continuous-valued annotations (analogous to Figure 3b). Results are
285 reported in Figure 4b and Table S16. We observed strong concordance, with a slope of 1.01
286 (correlation of 0.75) across the 53 SEG annotations. This implies that the depletions of
287 $\lambda^2(C)$ within SEG annotations are explained by corresponding values of continuous-valued
288 annotations.

289 In summary, our results show that causal disease effect sizes are more population-specific
290 in regions surrounding specifically expressed genes. This effect was strongest in tissues im-
291 pacted by positive selection (as opposed to negative selection), suggesting a possible connec-
292 tion between positive selection and population-specific causal effect sizes (see Discussion).

10

Discussion

²⁹⁴ We developed a new method (S-LDXR) for stratifying squared trans-ethnic genetic cor-
²⁹⁵ relation across functional categories of SNPs that yields approximately unbiased estimates
²⁹⁶ in extensive simulations. By applying S-LDXR to East Asian and European summary statis-
²⁹⁷ tics across 30 diseases and complex traits, we determined that SNPs with high background
²⁹⁸ selection statistic[27] have substantially lower squared trans-ethnic genetic correlation (vs.
²⁹⁹ the genome-wide average), implying that causal effect sizes are more population-specific.
³⁰⁰ Accordingly, squared trans-ethnic genetic correlations were substantially lower for SNPs in
³⁰¹ many functional categories. In analyses of specifically expressed gene annotations, we ob-
³⁰² served substantial depletion of squared trans-ethnic genetic correlation for SNPs near skin
³⁰³ and immune-related genes, which are strongly impacted by recent positive selection, but not
³⁰⁴ for SNPs near brain genes.

³⁰⁵ Reductions in trans-ethnic genetic correlation have several possible underlying expla-
³⁰⁶ nations, including gene-environment (G×E) interaction, gene-gene (G×G) interaction, and
³⁰⁷ dominance variation (but not differences in heritability across populations, which would
³⁰⁸ not affect trans-ethnic genetic correlation and were not observed in our study). Given the
³⁰⁹ increasing evidence of the role of G×E interaction in complex trait architectures,[41] and ev-
³¹⁰ idence that G×G interaction and dominance variation explain limited heritability,[42–44] we
³¹¹ hypothesize that depletions of squared trans-ethnic genetic correlation in the top quintile of
³¹² background selection statistic and in functionally important regions may be primarily at-
³¹³ tributable to stronger G×E interaction in these regions. Interestingly, a recent study on plas-
³¹⁴ ticity in Arabidopsis observed a similar phenomenon: lines with more extreme phenotypes
³¹⁵ exhibited stronger G×E interaction.[45] Distinguishing between stronger G×E interaction in
³¹⁶ regions impacted by selection and stronger G×E interaction in functionally important re-
³¹⁷ gions as possible explanations for our findings is a challenge, because functionally important
³¹⁸ regions are more strongly impacted by selection. To this end, we constructed an annotation
³¹⁹ that is similar to the background selection statistic but does not make use of recombination
³²⁰ rate, instead relying solely on a SNP's physical distance to the nearest exon (Methods).
³²¹ Applying S-LDXR to the 30 diseases and complex traits using a joint model incorporating
³²² baseline-LD-X model annotations and the nearest exon annotation, the background selec-
³²³ tion statistic remained highly conditionally informative for trans-ethnic genetic correlation,
³²⁴ whereas the nearest exon annotation was not conditionally informative (Table S17). This
³²⁵ result implicates stronger G×E interaction in regions with reduced effective population size
³²⁶ that are impacted by selection, and not just proximity to functional regions, in explaining
³²⁷ depletions of squared trans-ethnic genetic correlation; however, we emphasize that selection

11

acts on allele frequencies rather than causal effect sizes, and could help explain our findings only in conjunction with other explanations such as G×E interaction. Our results on specifically expressed genes implicate stronger G×E interaction near skin and immune genes and weaker G×E interaction near brain genes, potentially implicating positive selection (as opposed to negative selection). This conclusion is further supported by the lack of variation in squared trans-ethnic genetic correlation across genes in different deciles of probability of loss-of-function intolerance[46] (Methods, Figure S18, S19, Table S18). We conclude that depletions of squared trans-ethnic genetic correlation could potentially be explained by stronger G×E interaction at loci impacted by positive selection. We caution that other explanations are also possible; in particular, evolutionary modeling using an extension of the Eyre-Walker model[47] to two populations suggests that our results for the background selection statistic could also be consistent with negative selection (Supplementary Note, Figure S20, S21, Table S19). Additional information, such as genomic annotations that better distinguish different types of selection or data from additional diverse populations, may help elucidate the relationship between selection and population-specific causal effect sizes.

Our study has several implications. First, polygenic risk scores in non-European populations that make use of European training data[6,9] may be improved by reweighting SNPs based on the expected enrichment/depletion of squared trans-ethnic genetic correlation, helping to alleviate health disparities;[6,14,15] specifically, although the impact of population-specific LD patterns on trans-ethnic polygenic risk scores is well-documented,[6,9] population-specific causal effect sizes also merit thorough investigation. Second, modeling population-specific genetic architectures may improve trans-ethnic fine-mapping, moving beyond the standard assumption that all causal variants are shared across populations.[28,48] Third, modeling population-specific genetic architectures may also increase power in trans-ethnic meta-analysis,[49] e.g. by adapting MTAG[50] to two populations (instead of two traits). Fourth, it may be of interest to stratify G×E interaction effects[41] across genomic annotations. Fifth, the S-LDXR method could potentially be extended to stratify squared *cross-trait* genetic correlations[51] across genomic annotations.[52]

We note several limitations of this study. First, S-LDXR is designed for populations of homogeneous continental ancestry (e.g. East Asians and Europeans) and is not currently suitable for analysis of admixed populations[53] (analogous to LDSC and its published extensions[20,51,54]). However, a recently proposed extension of LDSC to admixed populations[55] could be incorporated into S-LDXR, enabling its application to the growing set of large studies in admixed populations.[10] Second, since S-LDXR applies shrinkage to reduce standard error in estimating stratified squared trans-ethnic genetic correlation and its enrichment, estimates are slightly conservative – true depletions of squared trans-ethnic genetic correlation

12

in functionally important regions may be stronger than the estimated depletions. Third, the specifically expressed gene (SEG) annotations analyzed in this study are defined primarily based on gene expression measurements of Europeans.[23] However, genetic architectures of gene expression differ across diverse populations.[12,56,57] Thus, SEG annotations derived from gene expression data from diverse populations may provide additional insights into population-specific causal effect sizes. Fourth, we restricted our analyses to SNPs that were relatively common (MAF>5%) in both populations, due to the lack of a large LD reference panel for East Asians. Extending our analyses to lower-frequency SNPs may provide further insights into the role of negative selection in shaping population-specific genetic architectures, given the particular importance of negative selection for low-frequency SNPs.[58] Fifth, we did not consider population-specific variants in our analyses, due to the difficulty in defining trans-ethnic genetic correlation for population-specific variants;[2,5] a recent study[59] has reported that population-specific variants substantially limit trans-ethnic genetic risk prediction accuracy. Sixth, estimates of genome-wide trans-ethnic genetic correlation may be confounded by different trait definitions or diagnostic criteria in the two populations, particularly for major depressive disorder. However, this would not impact estimates of enrichment/depletion of squared trans-ethnic genetic correlation ($\lambda^2(C)$), which is defined relative to genome-wide values. Seventh, we have not pinpointed the exact underlying phenomena (e.g. environmental heterogeneity coupled with gene-environment interaction) that lead to population-specific causal disease effect sizes at functionally important regions. Despite these limitations, our study provides an improved understanding of the underlying biology that contribute to population-specific causal effect sizes, and highlights the need for increasing diversity in genetic studies.

URLs

- S-LDXR software: https://github.com/huwenboshi/s-ldxr/
- Python code for simulating GWAS summary statistics: https://github.com/huwenboshi/s-ldxr-sim/
- baseline-LD-X model annotations and LD scores: https://data.broadinstitute.org/alkesgroup/LDSCORE/baseline-LD-X/
- Distance to nearest exon annotation and LD scores: https://data.broadinstitute.org/alkesgroup/LDSCORE/baseline-LD-X/
- baseline-LD model annotations: https://data.broadinstitute.org/alkesgroup/LDSCORE/readme_baseline_versions
- 1000 Genomes Project: https://www.internationalgenome.org/
- PLINK2: https://www.cog-genomics.org/plink/2.0/
- HAPGEN2: https://mathgen.stats.ox.ac.uk/genetics_software/hapgen/hapgen2.html
- UCSC Genome Browser: https://genome.ucsc.edu/
- Exome Aggregation Consortium (ExAC): https://exac.broadinstitute.org/

14

Methods

Definition of stratified squared trans-ethnic genetic correlation

We model a complex phenotype in two populations using linear models, $\boldsymbol{Y}_1 = \boldsymbol{X}_1\boldsymbol{\beta}_1 + \boldsymbol{\epsilon}_1$ and $\boldsymbol{Y}_2 = \boldsymbol{X}_2\boldsymbol{\beta}_2 + \boldsymbol{\epsilon}_2$, where $\boldsymbol{Y}_1$ and $\boldsymbol{Y}_2$ are vectors of phenotype measurements of population 1 and population 2 with sample size N_1 and N_2, respectively; $\boldsymbol{X}_1$ and $\boldsymbol{X}_2$ are mean-centered *but not normalized* genotype matrices at M SNPs in the two populations; $\boldsymbol{\beta}_1$ and $\boldsymbol{\beta}_2$ are *per-allele causal* effect sizes of the M SNPs; and $\boldsymbol{\epsilon}_1$ and $\boldsymbol{\epsilon}_2$ are environmental effects in the two populations. We assume that in each population, genotypes, causal effect sizes, and environmental effects are independent from each other. We assume that the per-allele effect size of SNP j in the two populations has variance and covariance,

$$\mathrm{Var}[\beta_{1j}] = \sum_C a_C(j)\tau_{1C}, \ \mathrm{Var}[\beta_{2j}] = \sum_C a_C(j)\tau_{2C},$$
$$\mathrm{Cov}[\beta_{1j}, \beta_{2j}] = \sum_C a_C(j)\theta_C, \tag{3}$$

where $a_C(j)$ is the value of SNP j for annotation C, which can be binary or continuous-valued; τ_{1C} and τ_{2C} are the net contribution of annotation C to the variance of β_{1j} and β_{2j}, respectively; and θ_C is the net contribution of annotation C to the covariance of β_{1j} and β_{2j}.

We define stratified trans-ethnic genetic correlation of a binary annotation C (e.g. functional annotations[20] or quintiles of continuous-valued annotations[21]) as,

$$r_g(C) = \frac{\rho_g(C)}{\sqrt{h_{g1}^2(C)}\sqrt{h_{g2}^2(C)}}, \tag{4}$$

where $\rho_g(C) = \sum_{j \in C} \mathrm{Cov}[\beta_{1j}, \beta_{2j}] = \sum_{j \in C} \sum_{C'} a_{C'}(j)\theta_{C'}$ is the trans-ethnic genetic covariance of annotation C; and $h_{gp}^2(C) = \sum_{j \in C} \mathrm{Var}[\beta_{pj}] = \sum_{j \in C} \sum_{C'} a_{C'}(j)\tau_{pC'}$ is the heritability (sum of per-SNP variance of causal effect sizes) of annotation C in population p. Here, C' includes both binary and continuous-valued annotations. Since estimates of $h_{gp}^2(C)$ can be noisy (possibly negative), we estimate *squared* stratified trans-ethnic genetic correlation,

$$r_g^2(C) = \frac{\rho_g^2(C)}{h_{g1}^2(C)h_{g2}^2(C)}, \tag{5}$$

to avoid bias or undefined values in the square root. In this work, we only estimate $r_g^2(C)$ for SNPs with minor allele frequency (MAF) greater than 5% in both populations. To assess whether causal effect sizes are more or less correlated for SNPs in annotation C compared

15

426 with the genome-wide average, r_g^2, we define the enrichment/depletion of stratified squared
427 trans-ethnic genetic correlation as

$$\lambda^2(C) = \frac{r_g^2(C)}{r_g^2}. \tag{6}$$

428 We meta-analyze $\lambda^2(C)$ instead of $r_g^2(C)$ across diseases and complex traits. We note that
429 the average value of $\lambda^2(C)$ across quintiles of continuous-valued annotations is not necessarily
430 equal to 1, as squared trans-ethnic genetic correlation is a non-linear quantity.

S-LDXR method

432 S-LDXR is conceptually related to stratified LD score regression[20,21] (S-LDSC), a method
433 for stratifying heritability from GWAS summary statistics, to two populations. The S-LDSC
434 method determines that a category of SNPs is enriched for heritability if SNPs with high
435 LD to that category have higher expected χ^2 statistic than SNPs with low LD to that cate-
436 gory. Analogously, the S-LDXR method determines that a category of SNPs is enriched for
437 trans-ethnic genetic covariance if SNPs with high LD to that category have higher expected
438 product of Z-scores than SNPs with low LD to that category.

439 S-LDXR relies on the regression equation

$$\mathrm{E}[Z_{1j}Z_{2j}] = \sqrt{N_1 N_2} \sum_C \ell_\times(j, C)\theta_C \tag{7}$$

440 to estimate θ_C, where Z_{pj} is the Z-score of SNP j in population p; $\ell_\times(j, C) = \sum_k r_{1jk} r_{2jk} \sigma_{1j} \sigma_{2j} a_C(k)$
441 is the trans-ethnic LD score of SNP j with respect to annotation C, whose value for SNP k,
442 $a_C(k)$, can be either binary or continuous; r_{pjk} is the LD between SNP j and k in population
443 p; and σ_{pj} is the standard deviation of SNP j in population p. We obtain unbiased estimates
444 of $\ell_\times(j, C)$ using genotype data of 481 East Asian and 489 European samples in the 1000
445 Genomes Project.[16] To account for heteroscedasticity and increase statistical efficiency, we
446 use weighted least square regression to estimate θ_C. We include only well-imputed (impu-
447 tation INFO>0.9) and common (MAF>5% in both populations) SNPs that are present in
448 HapMap 3[60] in the regression, as in our previous work.[20,51,54] We use regression equations
449 analogous to those described in ref.[20] to estimate τ_{1C} and τ_{2C}.

450 Let $\hat{\tau}_{1C}$, $\hat{\tau}_{1C}$, and $\hat{\theta}_C$ be the estimates of τ_{1C}, τ_{1C}, and θ_C, respectively. For each binary
451 annotation C, we estimate the stratified heritability of annotation C in each population,

16

452 $h_{g1}^2(C)$ and $h_{g2}^2(C)$, and trans-ethnic genetic covariance, $\rho_g(C)$, as

$$\hat{h}_{g2}^2(C) = \sum_{j \in C} \sum_{C'} a_{jC'} \hat{\tau}_{2C'}, \ \hat{h}_{g1}^2(C) = \sum_{j \in C} \sum_{C'} a_{jC'} \hat{\tau}_{1C'}, \ \hat{\rho}_g(C) = \sum_{j \in C} \sum_{C'} a_{jC'} \hat{\theta}_{C'}, \tag{8}$$

453 respectively, using coefficients ($\tau_{1C'}$, $\tau_{2C'}$, and $\theta_{C'}$) of both binary and continuous-valued
454 annotations. We then estimate $r_g^2(C)$ as

$$\hat{r}_g^2(C) = \frac{\hat{\rho}_g^2(C) - \hat{\text{S.E.}}^2[\hat{\rho}_g(C)]}{\hat{h}_{g1}^2(C)\hat{h}_{g2}^2(C) - \hat{\text{Cov}}[\hat{h}_{g1}^2(C), \hat{h}_{g2}^2(C)]} - \hat{\text{bias}}(C), \tag{9}$$

455 where $\hat{\text{bias}}(C)$ is obtained using bootstrap to correct for bias in estimating the ratio.[24] We
456 do not constrain the estimate of $r_g^2(C)$ to its plausible range of $[-1, 1]$ to be unbiased.
457 Subsequently, we obtain enrichment of stratified squared trans-ethnic genetic correlation as

$$\hat{\lambda}^2(C) = \frac{\hat{r}_g^2(C)}{\hat{r}_g^2}, \tag{10}$$

458 where $\hat{r}_g^2$ is the estimate of genome-wide squared trans-ethnic genetic correlation r_g^2. We use
459 block jackknife over 200 non-overlapping and equally sized blocks to obtain standard error
460 of all estimates. The standard error of $\lambda^2(C)$ typically depends on sample size of the GWAS
461 and overall heritability of annotation C in the two populations (i.e. $h_{g1}^2(C)$ and $h_{g2}^2(C)$).

462   To assess the informativeness of each annotation in explaining disease heritability and
463 trans-ethnic genetic covariance, we define standardized annotation effect size on heritability
464 and trans-ethnic genetic covariance for each annotation C analogous to ref.[21],

$$\tau_{1C}^* = \frac{Mh_{g1}^2}{h_{g1}^2(C)} \times \sigma_C \times \tau_{1C}, \ \tau_{2C}^* = \frac{Mh_{g2}^2}{h_{g2}^2(C)} \times \sigma_C \times \tau_{2C},$$
$$\theta_C^* = \frac{M\rho_g}{\rho_g(C)} \times \sigma_C \times \theta_C, \tag{11}$$

465 where τ_{1C}^*, τ_{2C}^*, and θ_C^* represent proportionate change in per-SNP heritability in population
466 1 and 2 and trans-ethnic genetic covariance, respectively, per standard deviation increase in
467 annotation C; τ_{1C}, τ_{2C}, and θ_C are the corresponding unstandardized effect sizes, defined in
468 Equation (3); and σ_C is the standard deviation of annotation C.

469   We provide a more detailed description of the method, including derivations of the
470 regression equation and unbiased estimators of the LD scores, in the **Supplementary Note**.

17

S-LDXR shrinkage estimator

Estimates of $r_g^2(C)$ can be imprecise with large standard errors if the denominator, $h_{g1}^2(C)h_{g2}^2(C)$, is close to zero and noisily estimated. This is especially the case for annotations of small size ($< 1\%$ SNPs). We introduce a shrinkage estimator to reduce the standard error in estimating $r_g^2(C)$.

Briefly, we shrink the estimated per-SNP heritability and trans-ethnic genetic covariance of annotation C towards the genome-wide averages, which are usually estimated with smaller standard errors, prior to estimating $r_g^2(C)$. In detail, let M_C be the number of SNPs in annotation C, we shrink $\frac{\hat{h}_{1g}^2(C)}{M_C}$, $\frac{\hat{h}_{2g}^2(C)}{M_C}$, and $\frac{\hat{\rho}_g(C)}{M_C}$ towards $\frac{\hat{h}_{1g}^2}{M}$, $\frac{\hat{h}_{2g}^2}{M}$, and $\frac{\hat{\rho}_g}{M}$, respectively, where $\hat{h}_{g1}^2$, $\hat{h}_{g2}^2$, $\hat{\rho}_g$ are the genome-wide estimates, and M the total number of SNPs. We obtain the shrinkage as follows. Let $\gamma_1 = 1/\left(1 + \alpha\frac{\mathrm{Var}\left[\hat{h}_{g1}^2(C)\right]}{\mathrm{Var}\left[\hat{h}_{g1}^2\right]}\frac{M}{M_C}\right)$, $\gamma_2 = 1/\left(1 + \alpha\frac{\mathrm{Var}\left[\hat{h}_{g2}^2(C)\right]}{\mathrm{Var}\left[\hat{h}_{g2}^2\right]}\frac{M}{M_C}\right)$, and $\gamma_3 = 1/\left(1 + \alpha\frac{\mathrm{Var}[\hat{\rho}_g(C)]}{\mathrm{Var}[\hat{\rho}_g]}\frac{M}{M_C}\right)$ be the shrinkage obtained separately for $\hat{h}_{g1}^2(C)$, $\hat{h}_{g2}^2(C)$ and $\hat{\rho}_g(C)$, respectively, where $\alpha \in [0,1]$ is the shrinkage parameter adjusting magnitude of shrinkage. We then choose the most stringent shrinkage, $\gamma = \min\{\gamma_1, \gamma_2, \gamma_3\}$, as the final shared shrinkage for both heritability and trans-ethnic genetic covariance.

We shrink heritability and trans-ethnic genetic covariance of annotation C using γ as, $\bar{h}_{g1}^2(C) = M_C\left(\gamma\frac{\hat{h}_{g1}^2(C)}{M_C} + (1-\gamma)\frac{\hat{h}_{g1}^2}{M}\right)$, $\bar{h}_{g2}^2(C) = M_C\left(\gamma\frac{\hat{h}_{g2}^2(C)}{M_C} + (1-\gamma)\frac{\hat{h}_{g2}^2}{M}\right)$, and $\bar{\rho}_g(C) = M_C\left(\gamma\frac{\hat{\rho}_g(C)}{M_C} + (1-\gamma)\frac{\hat{\rho}_g}{M}\right)$, where $\bar{h}_{g1}^2(C)$, $\bar{h}_{g2}^2(C)$, and $\bar{\rho}_g(C)$ are the shrunk counterparts of $\hat{h}_{g1}^2(C)$, $\hat{h}_{g2}^2(C)$, and $\hat{\rho}_g(C)$, respectively. We shrink $\hat{r}_g^2(C)$ by substituting $\hat{h}_{g1}^2(C)$, $\hat{h}_{g2}^2(C)$, and $\hat{\rho}_g(C)$ with $\bar{h}_{g1}^2(C)$, $\bar{h}_{g2}^2(C)$, $\bar{\rho}_g(C)$, respectively, in Equation (9), to obtain its shrunk counterpart, $\bar{r}_g^2(C)$. Finally, we shrink $\hat{\lambda}^2(C)$, by plugging in $\bar{r}_g^2(C)$ in Equation (10) to obtain its shrunk counterpart, $\bar{\lambda}^2(C)$. We recommend $\alpha = 0.5$ as the default shrinkage parameter value, as this value provides robust estimates of $\lambda^2(C)$ in simulations.

Baseline-LD-X model

We include a total of 54 binary functional annotations in the baseline-LD-X model. These include 53 annotations introduced in ref.,[20] which consists of 28 main annotations including conserved annotations (e.g. Coding, Conserved) and epigenomic annotations (e.g. H3K27ac, DHS, Enhancer) derived from ENCODE[61] and Roadmap,[62] 24 500-base-pair-extended main annotations, and 1 annotation containing all SNPs. We note that although chromatin accessibility can be population-specific, the fraction of such regions is small.[63] Following ref,[21] we created an additional annotation for all genomic positions with number of rejected substitutions[64] greater than 4. Further information for all functional annotations

18

included in the baseline-LD-X model is provided in Table S1a.

We also include a total of 8 continuous-valued annotations in the baseline-LD-X model. First, we include 5 continuous-valued annotations introduced in ref.[21] (see URLs), without modification: background selection statistic,[27] CpG content (within a ± 50 kb window), GERP (number of substitutation) score,[64] nucleotide diversity (within a ± 10 kb window), and Oxford map recombination rate (within a ± 10 kb window).[65] Second, we include 2 minor allele frequency (MAF) adjusted annotations introduced in ref.,[21] with modification: level of LD (LLD) and predicted allele age. We created analogous annotations applicable to both East Asian and European populations. To create an analogous LLD annotation, we estimated LD scores for each population using LDSC,[54] took the average across populations, and then quantile-normalized the average LD scores using 10 average MAF bins. We call this annotation "average level of LD". To create analogous predicted allele age annotation, we quantile-normalized allele age estimated by ARGweaver[66] across 54 multi-ethnic genomes using 10 average MAF bins. Finally, we include 1 continuous-valued annotation based on F_{ST} estimated by PLINK2,[67] which implements the Weir & Cockerham estimator of F_{ST}.[68] Further information for all continuous-valued annotations included in the baseline-LD-X model is provided in Table S1b.

Code and data availability

Python code implementing S-LDXR is available at https://github.com/huwenboshi/s-ldxr. Python code for simulating GWAS summary statistics under the baseline-LD-X model is available at https://github.com/huwenboshi/s-ldxr-sim. baseline-LD-X model annotations and LD scores are available at https://data.broadinstitute.org/alkesgroup/LDSCORE/baseline-LD-X/.

Simulations

We used simulated East Asian (EAS) and European (EUR) genotype data to assess the performance our method, as we did not have access to real EAS genotype data at sufficient sample size to perform simulations with real genotypes. We simulated genotype data for 100,000 East-Asian-like and 100,000 European-like individuals using HAPGEN2[25] (see URLs), starting from phased haplotypes of 481 East Asians and 489 Europeans individuals available in the 1000 Genomes Project[16] (see URLs), restricting to ∼2.5 million SNPs on chromosome $1-3$ with minor allele count greater than 5 in either population. Since excessive relatedness arose from HAPGEN2 simulations,[2] we used PLINK2[67] (see URLs) to remove simulated individuals with genetic relatedness greater than 0.05. From the filtered set of

19

536 individuals, we randomly selected 500 individuals in each simulated population to serve as
537 reference panels, and used the remaining 35,378 East-Asian-like and 36,836 European-like
538 individuals to simulate GWAS summary statistics.

539   We performed both null simulations, where enrichment of squared trans-ethnic genetic
540 correlation, $\lambda^2(C)$, is 1 across all functional annotations, and causal simulations, where
541 $\lambda^2(C)$ varies across annotations, under various degrees of polygenicity (1%, 10%, and 100%
542 causal SNPs). In the null simulations, we set τ_{1C}, τ_{2C}, θ_C to be the meta-analyzed τ_C in
543 real-data analyses of EAS GWASs, and followed Equation (3) to obtain variance, $\mathrm{Var}[\beta_{1j}]$
544 and $\mathrm{Var}[\beta_{2j}]$, and covariance, $\mathrm{Cov}[\beta_{1j}, \beta_{2j}]$, of per-SNP causal effect sizes β_{1j}, β_{2j}, setting
545 all negative per-SNP variance and covariance to 0. In the causal simulations, we directly
546 specified per-SNP causal effect size variances and covariances using self-devised τ_{1C}, τ_{2C}, and
547 θ_C coefficients, to attain $\lambda^2(C) \neq 1$, as these were difficult to attain using the coefficients
548 from analyses of real traits.

549   We randomly selected a subset of SNPs to be causal for both populations, and set
550 $\mathrm{Var}[\beta_{1j}]$, $\mathrm{Var}[\beta_{2j}]$, and $\mathrm{Cov}[\beta_{1j}, \beta_{2j}]$ to be 0 for all remaining non-causal SNPs. We scaled
551 the trans-ethnic genetic covariance to attain a desired genome-wide r_g. Next, we drew
552 causal effect sizes of each causal SNP j in the two populations from the bi-variate Gaussian
553 distribution,

$$\begin{bmatrix} \beta_{1j} \\ \beta_{2j} \end{bmatrix} \sim N\left(\begin{bmatrix} 0 \\ 0 \end{bmatrix}, \begin{bmatrix} \mathrm{Var}[\beta_{1j}] & \mathrm{Cov}[\beta_{1j}, \beta_{2j}] \\ \mathrm{Cov}[\beta_{1j}, \beta_{2j}] & \mathrm{Var}[\beta_{2j}] \end{bmatrix} \right), \tag{12}$$

554 and scaled the drawn effect sizes to match the desired total heritability and trans-ethnic
555 genetic covariance. We simulated genetic component of the phenotype in population p as
556 $\boldsymbol{X}_p\boldsymbol{\beta}_p$, where $\boldsymbol{X}_p$ is column-centered genotype matrix, and drew environmental effects, $\boldsymbol{\epsilon}_p$,
557 from the Gaussian distribution, $N\left(0, 1 - \mathrm{Var}[\boldsymbol{X}_p\boldsymbol{\beta}_p]\right)$, such that the total phenotypic vari-
558 ance in each population is 1. Finally, we simulated GWAS summary association statistics
559 for population p, $\boldsymbol{Z}_p$, as $Z_{pj} = \frac{\boldsymbol{X}_{pj}^\intercal \boldsymbol{Y}_p}{\sqrt{N_p}\sigma_{pj}}$, where σ_{pj} is the standard deviation of SNP j in pop-
560 ulation p. We have publicly released Python code for simulating GWAS summary statistics
561 for 2 populations (see URLs).

Summary statistics for 30 diseases and complex traits

563   We analyzed GWAS summary statistics of 30 diseases and complex traits, primarily
564 from UK Biobank,[69] Biobank Japan,[19] and CONVERGE.[17] These include: atrial fibrillation
565 (AF),[70,71] age at menarche(AMN),[72,73] age at menopause (AMP),[72,73] basophil count(BASO),[19,74]
566 body mass index (BMI),[19,75] blood sugar(BS),[19,75] diastolic blood pressure (DBP),[19,75] eosinophil

20

567 count(EO),[19,75] estimated glomerular filtration rate (EGFR),[19,76] hemoglobin A1c(HBA1C),[19,75]
568 height (HEIGHT),[75,77] high density lipoprotein (HDL),[19,75] hemoglobin (HGB),[19,74] hemat-
569 ocrit (HTC),[19,74] low density lipoprotein (LDL),[19,75] lymphocyte count(LYMPH),[19,75] mean
570 corpuscular hemoglobin (MCH),[19,75] mean corpuscular hemoglobin concentration (MCHC),[19,74]
571 mean corpuscular volume (MCV),[19,74] major depressive disorder (MDD),[17,78] monocyte count
572 (MONO),[19,75] neutrophil count(NEUT),[19,74] platelet count (PLT),[19,75] rheumatoid arthri-
573 tis(RA),[79] red blood cell count (RBC),[19,75] systolic blood pressure (SBP),[19,75] type 2 di-
574 abetes (T2D),[80,81] total cholesterol (TC),[19,75] triglyceride (TG),[19,75] and white blood cell
575 count (WBC).[19,75] Further information for the GWAS summary statistics analyzed is pro-
576 vided in Table S10. In our main analyses, we performed random-effect meta-analysis to
577 aggregate results across all 30 diseases and complex traits. We also defined a set of 20
578 approximately independent diseases and complex traits with cross-trait r_g^2 (estimated us-
579 ing cross-trait LDSC[51]) less than 0.25 in both populations: AF, AMN, AMP, BASO, BMI,
580 EGFR, EO, HBA1C, HEIGHT, HTC, LYMPH, MCHC, MCV, MDD, NEUT, PLT, RA,
581 SBP, TC, TG.

Expected enrichment of stratified squared trans-ethnic genetic correlation from 8 continuous-valued annotations

584 To obtain expected enrichment of squared trans-ethnic genetic correlation of a binary
585 annotation C, $\lambda^2(C)$, from 8 continuous-valued annotations, we first fit the S-LDXR model
586 using these 8 annotations together with the base annotation for all SNPs, yielding coefficients,
587 $\tau_{1C'}$, $\tau_{2C'}$, and $\theta_{C'}$, for a total of 9 annotations. We then use Equation (3) to obtain per-SNP
588 variance and covariance of causal effect sizes, β_{1j} and β_{1j}, substituting τ_{1C}, τ_{2C}, θ_C with $\tau_{1C'}$,
589 $\tau_{2C'}$, and $\theta_{C'}$, respectively. We apply shrinkage with default parameter setting ($\alpha = 0.5$),
590 and use Equation (9) and (10) to obtain expected stratified squared trans-ethnic genetic
591 correlation, $r_g^2(C)$, and subsequently $\lambda^2(C)$.

Analysis of specifically expressed gene annotations

593 We obtained 53 specifically expressed gene (SEG) annotations, defined in ref.[23] as
594 ± 100k-base-pair regions surrounding genes specifically expressed in each of 53 GTEx[29] tis-
595 sues. A list of the SEG annotations is provided in Table S2. Correlations between SEG
596 annotations and the 8 continuous-valued annotations are reported in Figure S17 and Table
597 S2. Most SEG annotations are moderately correlated with the background selection statistic
598 and CpG content annotations.

₅₉₉ To test whether there is heterogeneity in enrichment of squared trans-ethnic genetic

₆₀₀ correlation, $\lambda^2(C)$, across the 53 SEG annotations, we first computed the average $\lambda^2(C)$

₆₀₁ across the 53 annotations, $\bar{\lambda}^2(C)$, using fixed-effect meta-analysis. We then computed the test

₆₀₂ statistic $\sum_{i=1}^{53} \frac{\left(\hat{\lambda}^2(C_i) - \bar{\lambda}^2(C_i)\right)^2}{\text{Var}[\hat{\lambda}^2(C_i)]}$, where C_i is the i-th SEG annotation, and $\hat{\lambda}^2(C_i)$ the estimated

₆₀₃ $\lambda^2(C)$. We computed a p-value for this test statistic based on a χ^2 distribution with 53

₆₀₄ degrees of freedom.

₆₀₅ Analysis of distance to nearest exon annotation

₆₀₆ We created a continuous-valued annotation, named "distance to nearest exon annota-

₆₀₇ tion", based on a SNP's physical distance (number of base pairs) to its nearest exon, using

₆₀₈ 233,254 exons defined on the UCSC genome browser[82] (see URLs). This annotation is mod-

₆₀₉ erately correlated with the background selection statistic annotation[21] ($R = -0.21$), defined

₆₁₀ as (1 - McVicker B statistic / 1000), where the McVicker B statistic quantifies a site's genetic

₆₁₁ distance to its nearest exon.[27] We have publicly released this annotation (see URLs).

₆₁₂ To assess the informativeness of functionally important regions versus regions impacted

₆₁₃ by selection in explaining the depletions of squared trans-ethnic genetic correlation, we ap-

₆₁₄ plied S-LDXR on the distance to nearest exon annotation together with the baseline-LD-X

₆₁₅ model annotations. We used both enrichment of squared trans-ethnic genetic correlation

₆₁₆ ($\lambda^2(C)$) and standardized annotation effect size (τ_{1C}^*, τ_{2C}^*, and θ_C^*) to assess informativeness.

₆₁₇ Analysis of probability of loss-of-function intolerance decile gene
₆₁₈ annotations

₆₁₉ We created 10 annotations based on genes in deciles of probability of being loss-of-

₆₂₀ function intolerant (pLI) (see URLs), defined as the probability of assigning a gene into

₆₂₁ haplosufficient regions, where protein-truncating variants are depleted.[46] Genes with high

₆₂₂ pLI (e.g. > 0.9) have higly constrained functionality, and therefore mutations in these genes

₆₂₃ are subject to negative selection. We included SNPs within a 100kb-base-pair window around

₆₂₄ each gene, following ref.[23] A correlation heat map between pLI decile gene annotations and

₆₂₅ the 8 continuous-valued annotations is provided in Figure S18. All pLI decile gene anno-

₆₂₆ tations are moderately correlated with the background selection statistic and CpG content

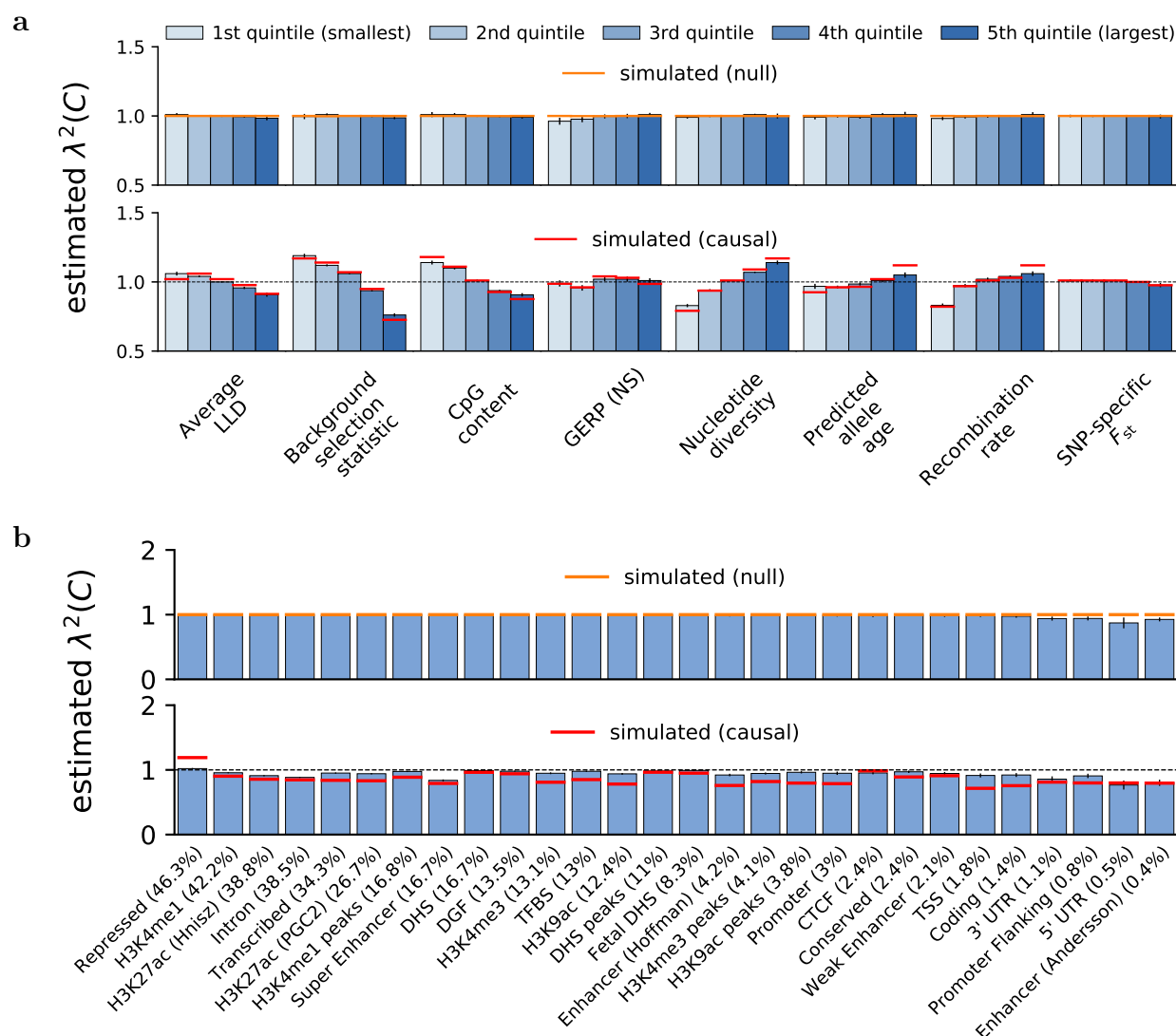₆₂₇ annotations.

Acknowledgements

Figure 1: **Accuracy of S-LDXR in null and causal simulations.** We report estimates of the enrichment/depletion of squared trans-ethnic genetic correlation ($\lambda^2(C)$) in both null and causal simulations, for (a) quintiles of 8 continuous-valued annotations and (b) 28 main binary annotations (sorted by proportion of SNPs, displayed in parentheses). Results are averaged across 1,000 simulations. Error bars denote $\pm 1.96\times$ standard error. Numerical results are reported in Table S5 and S8.
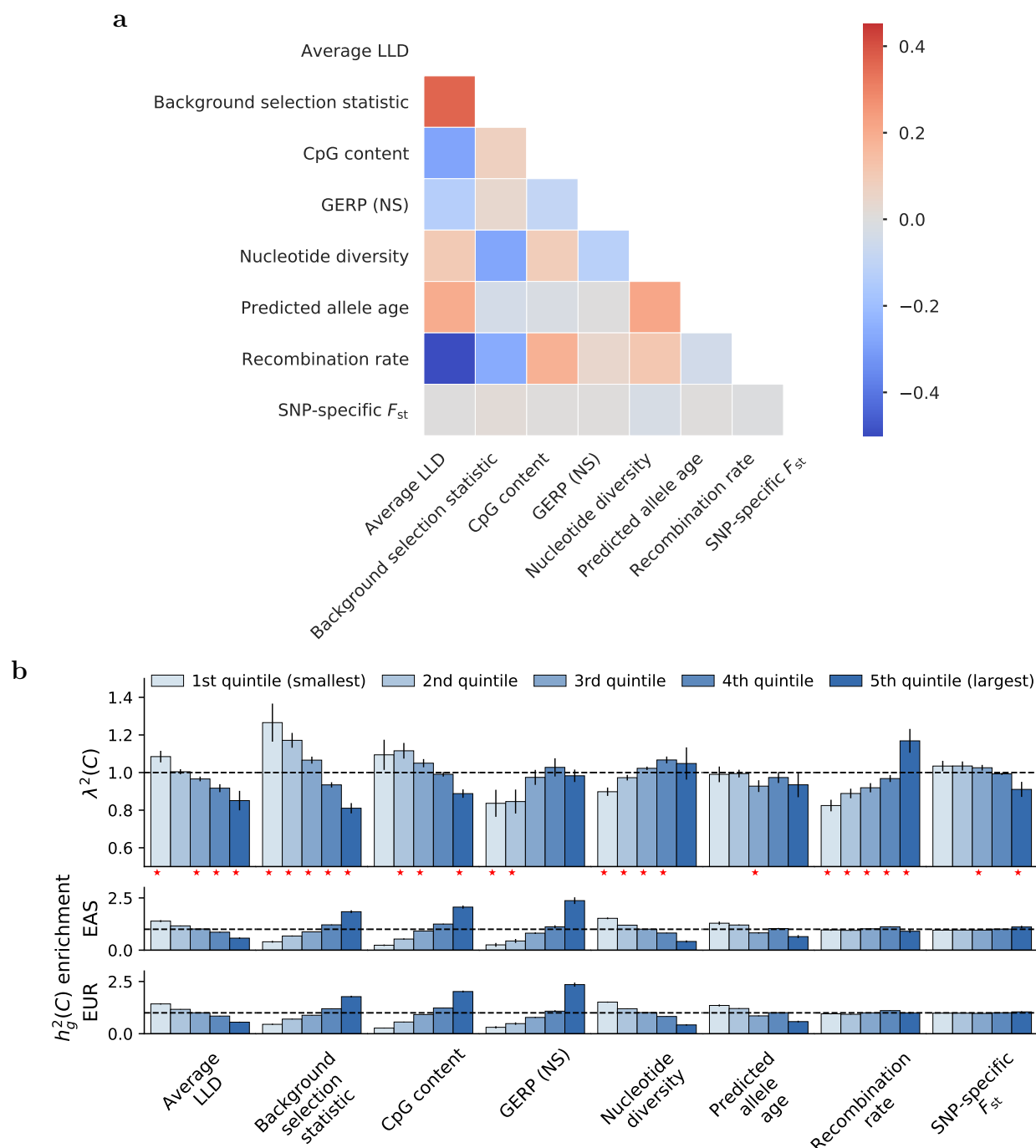
Figure 2: **S-LDXR results for quintiles of 8 continuous-valued annotations across 30 diseases and complex traits.** (a) We report correlations between each continuous-valued annotation; diagonal entries are not shown. Numerical results are reported in Table S1. (b) We report estimates of the enrichment/depletion of squared trans-ethnic genetic correlation ($\lambda^2(C)$), as well as population-specific estimates of heritability enrichment, for quintiles of each continuous-valued annotation. Results are meta-analyzed across 30 diseases and complex traits. Error bars denote $\pm 1.96\times$ standard error. Red stars ($\star$) denote two-tailed p<0.05/40. Numerical results are reported in Table S11.
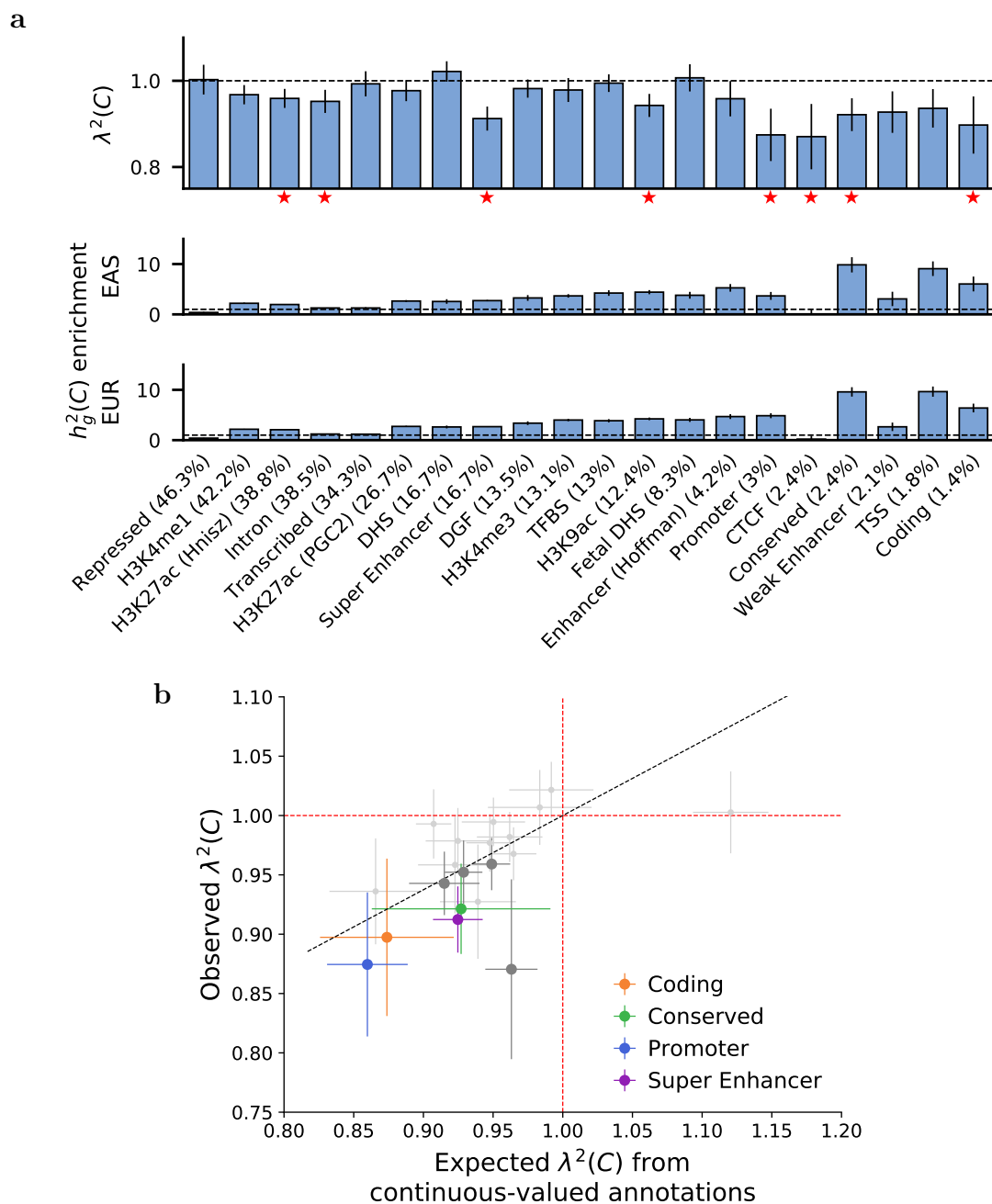
Figure 3: **S-LDXR results for 20 binary functional annotations across 30 diseases and complex traits.** (a) We report estimates of the enrichment/depletion of squared trans-ethnic genetic correlation ($\lambda^2(C)$), as well as population-specific estimates of heritability enrichment, for each binary annotation (sorted by proportion of SNPs, displayed in parentheses). Results are meta-analyzed across 30 diseases and complex traits. Error bars denote $\pm 1.96 \times$ standard error. Red stars ($\star$) denote two-tailed p<0.05/20. Numerical results are reported in Table S12. (b) We report observed $\lambda^2(C)$ vs. expected $\lambda^2(C)$ based on 8 continuous-valued annotations, for each binary annotation. Results are meta-analyzed across 30 diseases and complex traits. Error bars denote $\pm 1.96 \times$ standard error. Annotations for which $\lambda^2(C)$ is significantly different from 1 (p<0.05/20) are denoted in color (see legend) or dark gray. The dashed black line (slope=0.63) denotes a regression of observed $\lambda(C) - 1$ vs. expected $\lambda(C) - 1$ with intercept constrained to 0. Numerical results are reported in Table S13.
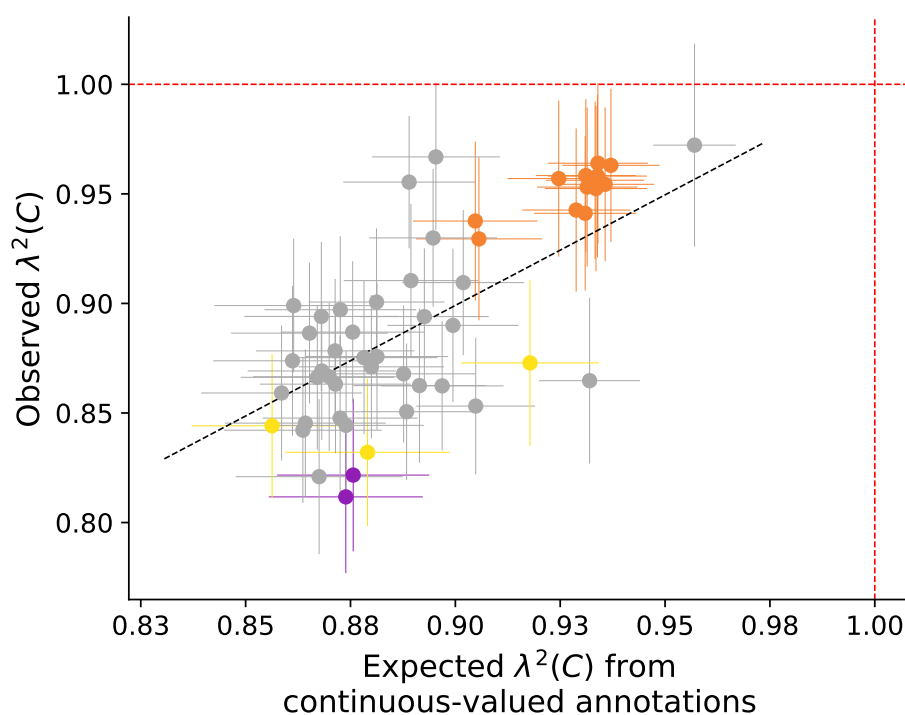
26
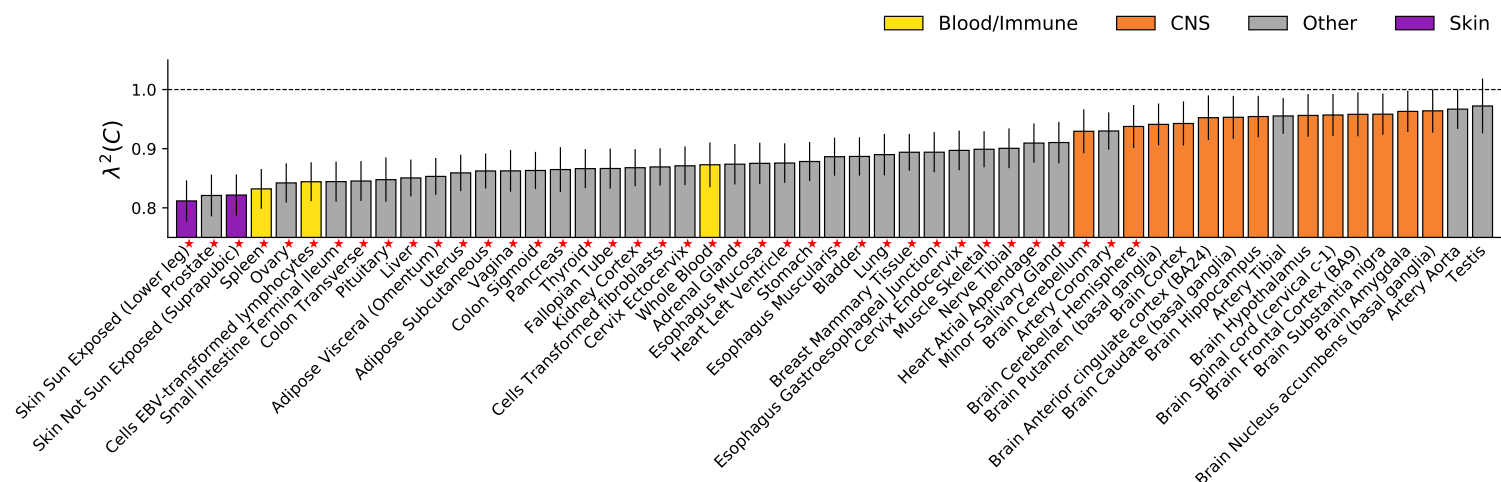
Figure 4: **S-LDXR results for 53 specifically expressed gene (SEG) annotations across 30 diseases and complex traits.** (a) We report estimates of the enrichment/depletion of squared trans-ethnic genetic correlation ($\lambda^2(C)$) for each SEG annotation (sorted by $\lambda^2(C)$). Results are meta-analyzed across 30 diseases and complex traits. Error bars denote $\pm 1.96\times$ standard error. Red stars ($\star$) denote two-tailed p<0.05/53. Numerical results are reported in Table S14. (b) We report observed $\lambda^2(C)$ vs. expected $\lambda^2(C)$ based on 8 continuous-valued annotations, for each SEG annotation. Results are meta-analyzed across 30 diseases and complex traits. Error bars denote $\pm 1.96\times$ standard error. Annotations are color-coded as in (a). The dashed black line (slope=1.01) denotes a regression of observed $\lambda(C) - 1$ vs. expected $\lambda(C) - 1$ with intercept constrained to 0. Numerical results and population-specific heritability enrichment estimates are reported in Table S16.

References

[1] Teresa R de Candia et al. "Additive genetic variation in schizophrenia risk is shared by populations of African and European descent". In: *The American Journal of Human Genetics* 93.3 (2013), pp. 463–470.

[2] Brielin C Brown et al. "Transethnic genetic-correlation estimates from summary statistics". In: *The American Journal of Human Genetics* 99.1 (2016), pp. 76–88.

[3] Nicholas Mancuso et al. "The contribution of rare variation to prostate cancer heritability". In: *Nature genetics* 48.1 (2016), p. 30.

[4] Masashi Ikeda et al. "Genome-Wide Association Study Detected Novel Susceptibility Genes for Schizophrenia and Shared Trans-Populations/Diseases Genetic Effect". In: *Schizophrenia bulletin* 45.4 (2018), pp. 824–834.

[5] Kevin J Galinsky et al. "Estimating cross-population genetic correlations of causal effect sizes". In: *Genetic epidemiology* 43.2 (2019), pp. 180–188.

[6] Alicia R Martin et al. "Clinical use of current polygenic risk scores may exacerbate health disparities". In: *Nature genetics* 51.4 (2019), p. 584.

[7] Christopher S Carlson et al. "Generalization and dilution of association results from European GWAS in populations of non-European ancestry: the PAGE study". In: *PLoS biology* 11.9 (2013), e1001661.

[8] Alicia R Martin et al. "Human demographic history impacts genetic risk prediction across diverse populations". In: *The American Journal of Human Genetics* 100.4 (2017), pp. 635–649.

[9] Carla Márquez-Luna et al. "Multiethnic polygenic risk scores improve risk prediction in diverse populations". In: *Genetic epidemiology* 41.8 (2017), pp. 811–823.

[10] Genevieve L Wojcik et al. "Genetic analyses of diverse populations improves discovery for complex traits". In: *Nature* (2019).

[11] L Duncan et al. "Analysis of polygenic risk score usage and performance in diverse human populations". In: *Nature Communications* 10.1 (2019), p. 3328.

[12] Kevin L Keys et al. "On the cross-population portability of gene expression prediction models". In: *bioRxiv* (2019), p. 552042.

[13] Sang Hong Lee et al. "Estimation of pleiotropy between complex diseases using single-nucleotide polymorphism-derived genomic relationships and restricted maximum likelihood". In: *Bioinformatics* 28.19 (2012), pp. 2540–2542.

[14] Giorgio Sirugo, Scott M Williams, and Sarah A Tishkoff. "The missing diversity in human genetic studies". In: *Cell* 177.1 (2019), pp. 26–31.

[15]   Deepti Gurdasani et al. "Genomics of disease risk in globally diverse populations". In: *Nature Reviews Genetics* (2019).

[16]   1000 Genomes Project Consortium et al. "A global reference for human genetic variation". In: *Nature* 526.7571 (2015), p. 68.

[17]   Na Cai et al. "Sparse whole-genome sequencing identifies two loci for major depressive disorder". In: *Nature* 523.7562 (2015), p. 588.

[18]   Akiko Nagai et al. "Overview of the BioBank Japan Project: study design and profile". In: *Journal of epidemiology* 27.Supplement_III (2017), S2–S8.

[19]   Masahiro Kanai et al. "Genetic analysis of quantitative traits in the Japanese population links cell types to complex human diseases". In: *Nature genetics* 50.3 (2018), p. 390.

[20]   Hilary K Finucane et al. "Partitioning heritability by functional annotation using genome-wide association summary statistics". In: *Nature genetics* 47.11 (2015), p. 1228.

[21]   Steven Gazal et al. "Linkage disequilibrium–dependent architecture of human complex traits shows action of negative selection". In: *Nature genetics* 49.10 (2017), p. 1421.

[22]   Steven Gazal et al. "Reconciling S-LDSC and LDAK functional enrichment estimates". In: *Nature genetics* 51.8 (2019), pp. 1202–1204.

[23]   Hilary K Finucane et al. "Heritability enrichment of specifically expressed genes identifies disease-relevant tissues and cell types". In: *Nature genetics* 50.4 (2018), p. 621.

[24]   James Durbin. "A note on the application of Quenouille's method of bias reduction to the estimation of ratios". In: *Biometrika* 46.3/4 (1959), pp. 477–480.

[25]   Zhan Su, Jonathan Marchini, and Peter Donnelly. "HAPGEN2: simulation of multiple disease SNPs". In: *Bioinformatics* 27.16 (2011), pp. 2304–2305.

[26]   Na Cai, Kenneth Kendler, and Jonathan Flint. "Minimal phenotyping yields GWAS hits of low specificity for major depression". In: *BioRxiv* (2018), p. 440735.

[27]   Graham McVicker et al. "Widespread genomic signatures of natural selection in hominid evolution". In: *PLoS genetics* 5.5 (2009), e1000471.

[28]   Gleb Kichaev and Bogdan Pasaniuc. "Leveraging functional-annotation data in trans-ethnic fine-mapping studies". In: *The American Journal of Human Genetics* 97.2 (2015), pp. 260–271.

[29]   GTEx Consortium et al. "Genetic effects on gene expression across human tissues". In: *Nature* 550.7675 (2017), p. 204.

[30]   Soumya Raychaudhuri et al. "Accurately assessing the risk of schizophrenia conferred by rare copy-number variation affecting genes with brain function". In: *PLoS genetics* 6.9 (2010), e1001097.

[31] Pardis C Sabeti et al. "Positive natural selection in the human lineage". In: *science* 312.5780 (2006), pp. 1614–1620.

[32] Rasmus Nielsen et al. "Recent and ongoing selection in the human genome". In: *Nature Reviews Genetics* 8.11 (2007), p. 857.

[33] John Novembre and Anna Di Rienzo. "Spatial patterns of variation due to natural selection in humans". In: *Nature Reviews Genetics* 10.11 (2009), p. 745.

[34] Kevin N Laland, John Odling-Smee, and Sean Myles. "How culture shaped the human genome: bringing genetics and the human sciences together". In: *Nature Reviews Genetics* 11.2 (2010), p. 137.

[35] Sandra Wilde et al. "Direct evidence for positive selection of skin, hair, and eye pigmentation in Europeans during the last 5,000 y". In: *Proceedings of the National Academy of Sciences* 111.13 (2014), pp. 4832–4837.

[36] Harald von Boehmer. "Positive selection of lymphocytes". In: *Cell* 76.2 (1994), pp. 219–228.

[37] Jian Zeng et al. "Signatures of negative selection in the genetic architecture of human complex traits". In: *Nature genetics* 50.5 (2018), p. 746.

[38] Luke J O'Connor et al. "Extreme Polygenicity of Complex Traits Is Explained by Negative Selection". In: *The American Journal of Human Genetics* (2019).

[39] Armin P Schoech et al. "Quantification of frequency-dependent genetic architectures in 25 UK Biobank traits reveals action of negative selection". In: *Nature communications* 10.1 (2019), p. 790.

[40] Krishna R Veeramah and Michael F Hammer. "The impact of whole-genome sequencing on the reconstruction of human population history". In: *Nature Reviews Genetics* 15.3 (2014), p. 149.

[41] Matthew R Robinson et al. "Genotype–covariate interaction effects and the heritability of adult body mass index". In: *Nature genetics* 49.8 (2017), p. 1174.

[42] William G Hill, Michael E Goddard, and Peter M Visscher. "Data and theory point to mainly additive genetic variance for complex traits". In: *PLoS genetics* 4.2 (2008), e1000008.

[43] Asko Mäki-Tanila and William G Hill. "Influence of gene interaction on complex trait variation with multilocus models". In: *Genetics* 198.1 (2014), pp. 355–367.

[44] Zhihong Zhu et al. "Dominance genetic variation contributes little to the missing heritability for human complex traits". In: *The American Journal of Human Genetics* 96.3 (2015), pp. 377–385.

[45] Maaike de Jong et al. "Natural variation in Arabidopsis shoot branching plasticity in response to nitrate supply affects fitness". In: *PLoS genetics* 15.9 (2019), e1008366.

[46] Monkol Lek et al. "Analysis of protein-coding genetic variation in 60,706 humans". In: *Nature* 536.7616 (2016), p. 285.

[47] Adam Eyre-Walker. "Genetic architecture of a complex trait and its implications for fitness and genome-wide association studies". In: *Proceedings of the National Academy of Sciences* (2010), p. 200906182.

[48] Reedik Mägi et al. "Trans-ethnic meta-regression of genome-wide association studies accounting for ancestry increases power for discovery and improves fine-mapping resolution". In: *Human molecular genetics* 26.18 (2017), pp. 3639–3650.

[49] Andrew P Morris. "Transethnic meta-analysis of genomewide association studies". In: *Genetic epidemiology* 35.8 (2011), pp. 809–822.

[50] Patrick Turley et al. "Multi-trait analysis of genome-wide association summary statistics using MTAG". In: *Nature genetics* 50.2 (2018), p. 229.

[51] Brendan Bulik-Sullivan et al. "An atlas of genetic correlations across human diseases and traits". In: *Nature genetics* 47.11 (2015), p. 1236.

[52] Qiongshi Lu et al. "A powerful approach to estimating annotation-stratified genetic covariance via GWAS summary statistics". In: *The American Journal of Human Genetics* 101.6 (2017), pp. 939–964.

[53] Michael F Seldin, Bogdan Pasaniuc, and Alkes L Price. "New approaches to disease mapping in admixed populations". In: *Nature Reviews Genetics* 12.8 (2011), p. 523.

[54] Brendan K Bulik-Sullivan et al. "LD Score regression distinguishes confounding from polygenicity in genome-wide association studies". In: *Nature genetics* 47.3 (2015), p. 291.

[55] Yang Luo et al. "Estimating heritability and its enrichment in tissue-specific gene sets in admixed populations". In: *bioRxiv* (2019), p. 503144.

[56] Alicia R Martin et al. "Transcriptome sequencing from diverse human populations reveals differentiated regulatory architecture". In: *PLoS genetics* 10.8 (2014), e1004549.

[57] Lauren S Mogil et al. "Genetic architecture of gene expression traits across diverse populations". In: *PLoS genetics* 14.8 (2018), e1007586.

[58] S Gazal et al. "Functional architecture of low-frequency variants highlights strength of negative selection across coding and non-coding annotations." In: *Nature genetics* 50.11 (2018), p. 1600.

[59] Arun Durvasula and Kirk E Lohmueller. "Negative selection on complex traits limits genetic risk prediction accuracy between populations". In: *bioRxiv* (2019), p. 721936.

[60] International HapMap 3 Consortium et al. "Integrating common and rare genetic variation in diverse human populations". In: *Nature* 467.7311 (2010), p. 52.

31

[61]   ENCODE Project Consortium et al. "An integrated encyclopedia of DNA elements in the human genome". In: *Nature* 489.7414 (2012), p. 57.

[62]   Anshul Kundaje et al. "Integrative analysis of 111 reference human epigenomes". In: *Nature* 518.7539 (2015), p. 317.

[63]   Maya Kasowski et al. "Extensive variation in chromatin states across humans". In: *Science* 342.6159 (2013), pp. 750–752.

[64]   Eugene V Davydov et al. "Identifying a high fraction of the human genome to be under selective constraint using GERP++". In: *PLoS computational biology* 6.12 (2010), e1001025.

[65]   Simon Myers et al. "A fine-scale map of recombination rates and hotspots across the human genome". In: *Science* 310.5746 (2005), pp. 321–324.

[66]   Matthew D Rasmussen et al. "Genome-wide inference of ancestral recombination graphs". In: *PLoS genetics* 10.5 (2014), e1004342.

[67]   Christopher C Chang et al. "Second-generation PLINK: rising to the challenge of larger and richer datasets". In: *Gigascience* 4.1 (2015), p. 7.

[68]   Bruce S Weir and C Clark Cockerham. "Estimating F-statistics for the analysis of population structure". In: *evolution* 38.6 (1984), pp. 1358–1370.

[69]   Clare Bycroft et al. "The UK Biobank resource with deep phenotyping and genomic data". In: *Nature* 562.7726 (2018), p. 203.

[70]   Siew-Kee Low et al. "Identification of six new genetic loci associated with atrial fibrillation in the Japanese population". In: *Nature genetics* 49.6 (2017), p. 953.

[71]   Jonas B Nielsen et al. "Biobank-driven genomic discovery yields new insight into atrial fibrillation biology". In: *Nature genetics* 50.9 (2018), p. 1234.

[72]   Momoko Horikoshi et al. "Elucidating the genetic architecture of reproductive ageing in the Japanese population". In: *Nature communications* 9.1 (2018), p. 1977.

[73]   Felix R Day et al. "Large-scale genomic analyses link reproductive aging to hypothalamic signaling, breast cancer susceptibility and BRCA1-mediated DNA repair". In: *Nature genetics* 47.11 (2015), p. 1294.

[74]   William J Astle et al. "The allelic landscape of human blood cell trait variation and links to common complex disease". In: *Cell* 167.5 (2016), pp. 1415–1429.

[75]   Po-Ru Loh et al. "Mixed-model association for biobank-scale datasets". In: *Nature genetics* 50.7 (2018), p. 906.

[76]   Cristian Pattaro et al. "Genetic associations at 53 loci highlight cell types and biological pathways relevant for kidney function". In: *Nature communications* 7 (2016), p. 10023.

[77]   Masato Akiyama et al. "Characterizing rare and low-frequency height-associated variants in the Japanese population". In: *Nature Communications* 10.1 (2019), pp. 1–11.

[78] Naomi R Wray et al. "Genome-wide association analyses identify 44 risk variants and refine the genetic architecture of major depression". In: *Nature genetics* 50.5 (2018), p. 668.

[79] Yukinori Okada et al. "Genetics of rheumatoid arthritis contributes to biology and drug discovery". In: *Nature* 506.7488 (2014), p. 376.

[80] Ken Suzuki et al. "Identification of 28 new susceptibility loci for type 2 diabetes in the Japanese population". In: *Nature genetics* 51.3 (2019), p. 379.

[81] Robert A Scott et al. "An expanded genome-wide association study of type 2 diabetes in Europeans". In: *Diabetes* 66.11 (2017), pp. 2888–2902.

[82] Donna Karolchik, Angie S Hinrichs, and W James Kent. "The UCSC genome browser". In: *Current protocols in bioinformatics* 40.1 (2012), pp. 1–4.